# Study on Bow Shape Optimization of Ultra Large Block Coefficient Ship and CFD Simulations of Initial and Optimized Hull Forms

by Aye Aye Mon* Kazuo Suzuki**, *Member*
*Takanori Hino**, Member*

**Summary**

The present paper describes a hull form improvement of innovative low-speed Ultra Large Block coefficient Ship (ULBS). A hull form optimization method for reducing wave-making resistance and wave-breaking at the bow using nonlinear programming method (NLP) based on the Rankine source method is discussed. In the optimization process, wave-making resistance coefficient, surface integrals of the square of free surface elevations and free surface disturbance function $D(x, y)$-values are selected as the objective functions. Bow-body shape is optimized under the prescribed design constraints based on the present method. Numerical examples are given for unconventional ULBS. The three improved hull forms for the corresponding objective functions are obtained by optimal designs which indicate that the objective functions are reduced distinctly. In order to verify the present optimization method based on the potential solver, the flow characteristics around the initial and bow optimized hull forms are analyzed by using Computational Fluid Dynamics (CFD) analysis based on the Navier-Stokes (NS) solver. Comparisons of the computed resistance coefficients, pressure and velocity distributions of the initial and bow optimized hull forms are presented. It is confirmed that simulation results based on the viscous flow solver show reasonable agreements with the numerical results based on the Rankine source method for the bow optimized hull forms.

## 1. Introduction

The world needs better, more Eco-friendly ships with large cargo capacity and low resistance as the use of maritime transportation has been increasing significantly. Considering these needs, the fresh and improved concepts of Ultra Large Block coefficient Ship (ULBS) are proposed as green ship technologies for energy saving and environmental conservations. Its concepts and study plans have been introduced[1]. ULBS is supposed to have very blunt hull forms with block coefficients larger than 0.95 and $L/B$ is smaller than 5 for large cargo capacity and to sail at low speed from 10 to 15 knots. For the practical applications of ULBS, it is necessary to carry out the various studies related to hull form improvements by using experimental and numerical analysis based on Computational Fluid Dynamics (CFD).

In the case of slowly moving blunt ships, usually wave-breaking occurs in front of the bow. From wave and wake measurements of tanker models, Baba[2] found that in the ballast condition a resistance component due to wave-breaking at the bow occupies a considerable portion of the total resistance. From the analytical calculations of semi-submerged ellipsoids, Baba[3] showed that the steeper waves give higher peak value of free surface disturbance function. It is considered that free surface disturbance function $D(x, y)$ may be used as a measure of wave-breaking inception and wave-breaking phenomena will be suppressed by reducing $D(x, y)$-values in front of the bow of blunt ships.

Therefore, the correlation between wave breaking and free surface disturbance function which is used as a numerical parameter for prediction of bow wave-breaking according to the Baba's low speed theory[3] was investigated by experimentally and numerically as one of the fundamental studies on ULBS hull form[1]. It has been concluded that the theoretical results based on wave-making resistance coefficients, surface integrals of the square of free surface elevation and free surface disturbance function have strong relations to experimental wave-breaking surface areas.

Since ULBS is an extremely blunt ship, it should be optimized to obtain a hull form with low wave-making resistance and small wave-breaking at the bow from the hydrodynamic point of view. In recent years, many researchers have discussed the hull form optimization methods with numerical flow solvers which can be used to evaluate the objective functions and hydrodynamic performances of ship hull form. For the purpose of the bow hull form optimizations based on these CFD approaches, the Navier-Stokes (NS) solver should be employed for the consideration of viscous effect, however, it would take a great amount of time for repeated grid generation and numerical computations during the whole optimization process. In order to avoid this inconvenience, a simplified method based on the potential solver which combines with nonlinear programming (NLP) technique is proposed for the present optimization problem. Although the simulation of wave-breaking is impossible by the potential flow solver, it is considered that the characteristics of

* Graduate School of Engineering, Yokohama National University
** Faculty of Engineering, Yokohama National University

Received 2nd June 2014

wave-breaking phenomena can be investigated based on the surface integral of the square of free surface disturbance function $D(x,y)$ because it has strong relations to wave-breaking surface area according to the previous study on ULBS[1]. Therefore, in the present study of bow shapes optimization, the wave-making resistance coefficient, the surface integral of the square of free surface elevations which is related to wave-making resistance and surface integral of the square of free surface disturbance function $D(x,y)$ which is related to bow wave-breaking surface area are taken as the objective functions.

In the first part of the present study, ULBS ($C_b = 0.9725$) is selected as the initial hull form to be optimized. SQP (Sequential Quadratic Programming) is employed as the NLP. The wave-making resistance coefficient and distributions of free surface elevations are evaluated by means of a Rankine source method. The distributions of free surface disturbance function $D(x,y)$-values are evaluated using the method proposed by Hess and Smith[4] according to Baba's low speed theory[3] for an indicator of wave-breaking. The examples of numerical optimization are provided for the ULBS hull form.

In the latter part of the present study, CFD analysis based on a viscous flow solver is applied to simulate the flow characteristics around the initial and bow optimized hull forms of the ULBS. Comparisons are made for computed resistance components, pressure and velocity distributions among the initial and bow optimized hull forms. The wave patterns and flow fields around the hull forms are presented.

## 2. Rankine Source Method

The Rankine source method is a numerical calculation method for wave-making resistance acting on the hull surface and wave elevations based on the double model flow with a free surface effect[5),6)]. The origin of the coordinate system is located in an undisturbed free surface at midship. The *x*- axis is considered positive in the direction of uniform fluid velocity *U* towards the aft, the *y*-axis extends to starboard and the *z*-axis is vertically upward as shown in Fig. 1.

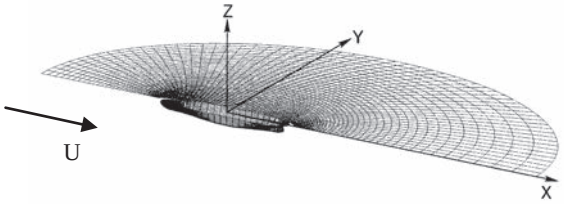


Fig. 1 Coordinate system and source panel arrangements.

In the Rankine source method, the fluid is considered inviscid and irrotational. The total velocity potential on the free surface $\phi$ is the sum of velocity potential due to double model flow, $\phi_0$ and the perturbed velocity potential representing the effect of free surface, $\phi_1$.

$$\phi = \phi_0 + \phi_1 \tag{1}$$

$$\phi_0(x,y,z) = Ux - \iint_{S_0} \sigma_0(x',y',z')\frac{1}{r_0}dz \tag{2}$$

$$\phi_1(x,y,z) = -\iint_{S_1} \sigma_1(x',y')\frac{1}{r_1}dx'dy' - \iint_{S_0} \Delta\sigma_0(x',y',z')\frac{1}{r_0}dS \tag{3}$$

where, $S_0$ is the hull surface of the double model, $S_1$ is the undisturbed free surface and

$$r_0 = \sqrt{(x-x')^2 + (y-y')^2 + (z-z')^2} \tag{4}$$

$$r_1 = \sqrt{(x-x')^2 + (y-y')^2 + z^2} \tag{5}$$

The hull surface boundary condition to be satisfied for the velocity potential is the normal velocity component on the hull surface must be zero. The velocity potentials in Eq. (3) are solved under the following hull surface conditions on $S_0$ and Dawson's double model linearized free surface condition on $S_1$.

$$\frac{\partial\phi_0}{\partial n} = 0,\ \frac{\partial\phi_1}{\partial n} = 0 \quad \text{on} \quad S_0 \tag{6}$$

$$\phi_{0l}^2\phi_{1ll} + 2\phi_{0l}\phi_{0ll}\phi_{1l} + g\phi_{1z} = -\phi_{0l}^2\phi_{0ll} \text{ on } S_1 \text{ and } z = 0 \tag{7}$$

In the free surface condition (Eq. (7)), *l* denotes a stream line direction on $S_1$ based on the double model flow.

The pressure around the hull can be determined from Bernoulli's equation by neglecting the higher order terms of $\phi_0$ and $\phi_1$. The equation can be expressed as follows:

$$p - p_0 = \frac{1}{2}\rho\left(U^2 - \phi_{0x}^2 - \phi_{0y}^2 - \phi_{0z}^2 - 2\phi_{0x}\phi_{1x} - 2\phi_{0y}\phi_{1y} - 2\phi_{0z}\phi_{1z}\right) \tag{8}$$

Then, the wave height of the free surface can be expressed as:

$$\zeta(x,y) = \frac{1}{2g}\left(U^2 - \phi_{0x}^2 - \phi_{0y}^2 - 2\phi_{0x}\phi_{1x} - 2\phi_{0y}\phi_{1y}\right) \tag{9}$$

where, $p_0$ is the atmospheric pressure and $g$ is the acceleration of gravity.

The wave-making resistance coefficient calculated by the Rankine source method is defined by

$$C_w = \frac{R_w}{\frac{1}{2}\rho U^2 L^2}, \quad R_w = -\iint_S p\, n_x\, dS \tag{10}$$

where, $R_w$ is wave-making resistance, $L$ is ship length between perpendiculars, $\rho$ is the density of water and $U$ is the ship speed, $n_x$ is the *x*-component of unit normal on the hull surface, $dS$ is the area of panel on the hull surface.

The integration of the square of free surface elevations can be evaluated by means of the Rankine source method using the elliptical panel arrangement on the free surface by Eq. (11).

$$I_{\zeta^2} = \int_0^{\infty}\int_{-\infty}^{-0.5L} \zeta^2(x,y)/L^2\ dxdy \tag{11}$$

After solving the source density distributions on the double model hull surface by using the Hess and Smith method[4] without a free surface effect, the distributions of free surface disturbance function $D(x,y)$ can be evaluated by means of Baba's low speed theory[3].

$$D(x,y) = \frac{\partial}{\partial x}\left[\phi_{0x}(x,y,0)\,\zeta_0(x,y)\right] + \frac{\partial}{\partial y}\left[\phi_{0y}(x,y,0)\,\zeta_0(x,y)\right] \tag{12}$$

where,

$$\zeta_0(x,y)=\frac{1}{2g}\left[U^2-\phi_{0x}^2(x,y,0)-\phi_{0y}^2(x,y,0)\right] \tag{13}$$

The value of numerical parameter $I_{D^2}$ can be obtained by calculating the free surface disturbance function $D(x,y)$ using the mathematical procedures described by Akima[7), 8)].

$$I_{D^2}=\int_0^{\infty}\int_{-\infty}^{-0.5L} D^2(x,y)/U^2\ dxdy \tag{14}$$

## 3. Optimizations of Bow Shapes of ULBS

### 3. 1 Optimization Method

The numerical optimization can be carried out systematically by iterative evaluations of an objective function as shown in Fig. 2. In this study, Sequential Quadratic Programming (SQP) is selected as the NLP to minimize the objective function under the prescribed design constraints. The robust SQP technique is widely used for solving optimization problems with constraints (NLP) and the detailed algorithms of SQP are described in the references [9),10)].

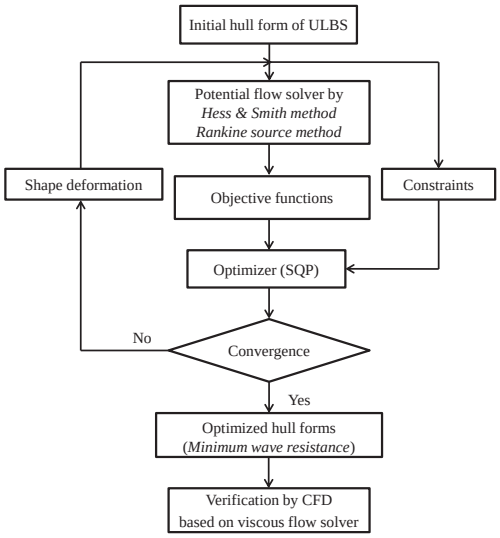


Fig. 2 Flow diagram of iterative optimization process.

### 3. 2 Design Variables and Hull Form Modification Function

The fore part of the hull form is taken as the scope of design modification region as shown in Fig. 3. In order to generate a new hull surface $y(x,z)$ from the initial hull surface $f_0(x,z)$ in the optimization process, the following hull surface deformation method suggested by Masuda et.al.[10), 11)] is introduced:

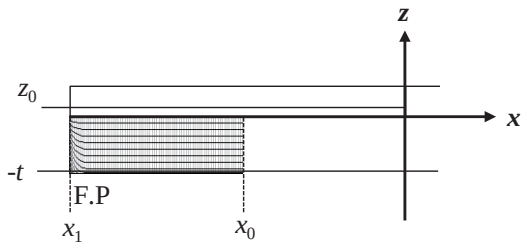


Fig. 3 Hull surface modification area.

$$y(x,z)=w(x)f_0(x,z) \tag{15}$$

$$w(x)=1-\sum_{i=0}^{N}a_i\left(\frac{x_1-x}{x_1-x_0}\right)^i \text{ on the selected water line} \tag{16}$$

The hull form modification function $w(x)$ is an N-th order polynomial function as shown in Eq. (16), which is defined in the modification region as $x_0\le x\le x_1$. The spline interpolation is used to get new frame lines on an arbitrary section from Eq. (16). In the optimization process, coefficients $a_i$ can be taken as design variables; however the following conditions should be imposed on $w(x)$ in Eq. (16):

$$\begin{aligned} &w(x)=1 \ \text{ at } \ x=x_0 \ \text{ and } \ x=x_1\\ &\frac{\partial w(x)}{\partial x}=0 \ \text{ at } \ x=x_1 \end{aligned} \tag{17}$$

From Eq. (17), coefficients $a_i$ satisfy such relations as

$$a_0=0,\ a_1=0,\ a_2=-\sum_{3}^{N}a_i \tag{18}$$

### 3. 3 Objective Functions

In the present study, according to the previous study on ULBS[1)], three objective functions based on Eqs. (10), (11) and (13), respectively to be minimized in the optimization processes are defined as follows:

(1) Wave-making resistance coefficient, $C_w$ :

$$Obj(1)=C_w=\frac{R_w}{\frac{1}{2}\rho U^2L^2},\quad R_w=-\iint_S p\,n_x\,dS \tag{19}$$

(2) The integration of square of wave elevation over free surface in front of bow, $I_{\zeta^2}$ :

$$Obj(2)=I_{\zeta^2}=\int_0^{\infty}\int_{-\infty}^{-0.5L}\zeta^2(x,y)/L^2\ dxdy \tag{20}$$

(3) The integration of the square of the value of free surface disturbance function $D(x,y)$ in front of the bow, $I_{D^2}$ :

$$Obj(3)=I_{D^2}=\int_0^{\infty}\int_{-\infty}^{-0.5L}D^2(x,y)/U^2\ dxdy \tag{21}$$

## 4. Results of Hull Form Optimization

The full hull form ULBS ($C_b$ =0.9725) is selected as the initial hull form to be optimized. The particulars of ULBS are shown in Table 1. The hull surface is divided into 3402 panels as shown in Fig 4. The free surface is divided into 4800 quadrilateral panels in the whole domain which starts from 1.5$L$ upstream to 2.5$L$ downstream ($L$=ship length) having the elliptical boundary, as shown in Fig. 5. No panels are arranged on the stern end and on the free surface near the stern. This treatment was used in the

previous study[1] and the wave-making resistance computation using Eq. (10) is only for the fore part of the hull. The pressure distributions on the bow hull surface cannot be affected by this treatment, because ULBS has long parallel body.

In the present optimization, 4th-order polynomials are assumed as $w(x)$ on five selected water lines, and then ten coefficients are chosen as design variables. The fore part of the hull form is selected as the scope of optimization design and the modification regions for the ULBS hull form under the optimization process are shown in Fig. 6.

The design conditions and constraints are shown in Table 2, in which Case 3 has different modification region and design constraints from Cases 1 and 2.

In this study, the trial calculations have been carried out for Case 3 with the same condition as Cases 1 and 2, also for Cases 1 and 2 with the same condition as Case 3. From the solutions of trial cases, it is observed that there is no optimal shape in Case 3 with the same condition as Cases 1 and 2 since the frame lines of the obtained hull form by *Obj*(3) are almost the same as those of the initial hull form. Therefore, the modification region of Case 3 is changed and the displacement volume constraint is also modified in accordance with the change of modification region.

It is also observed that the optimal solutions obtained by Cases 1 and 2 with the same condition as Case 3 are not much better than those obtained by Cases 1 and 2 with the current design conditions.

Based on those optimal solutions of all cases, the current two different design conditions and constraints of the optimization processes are presented in Table 2. $\nabla_0$, $\nabla$ are the displacement volumes of the initial and improved hulls, respectively and $B$ is the maximum breadth of the initial hull.

In the optimization cases, wave-making resistance coefficient and wave elevations are evaluated by the Rankine source method with the free surface effect (Case 1 and 2). The free surface disturbance function $D(x, y)$ is calculated by means of Baba's low speed theory[3] using the mathematical procedures described by Akima's method[7),8)] in addition to the Hess and Smith method[4] (Case 3).

Table 1 Particulars of ULBS hull form.

| Length ($L/L_{pp}$) | Breadth ($B/L_{pp}$) | Draft ($d/L_{pp}$) | Block coefficient | Design $F_n$ |
|---|---|---|---|---|
| 1.00 | 0.20 | 0.0667 | 0.9725 | 0.15 |

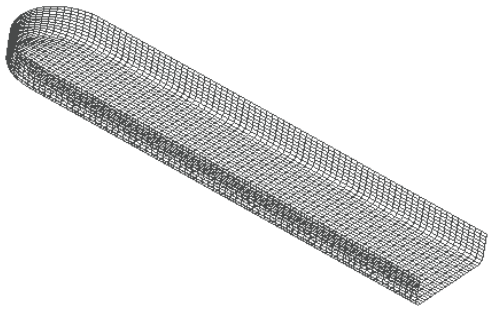

Fig. 4 Hull surface panel arrangements of ULBS.

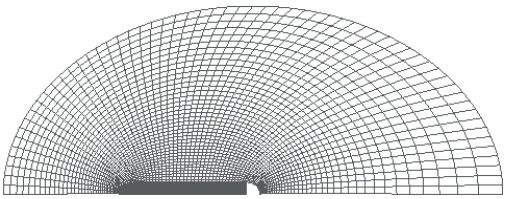

Fig. 5 Free surface and hull surface panel arrangements of ULBS.

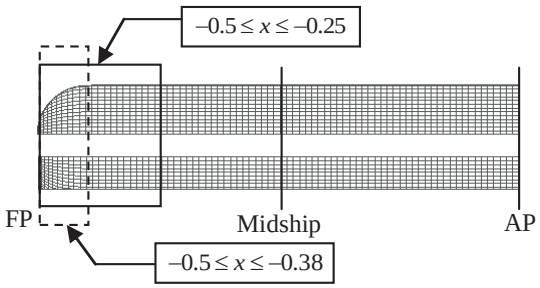


Fig. 6 Hull surface modification areas for the ULBS hull form.

Table 2 Design conditions and constraints for the ULBS hull.

| Case No. | Modification regions | Objective functions | Design Constraints |
|---|---|---|---|
| Case 1 | $-0.5 \le x \le -0.25$ | *Obj*(1) | $y(x,z) \ge 0$<br>$0.995\nabla_0 \le \nabla \le 1.05\nabla_0$<br>$y(x,z)_{\max} \le 1.0001 \times \frac{B}{2}$ |
| Case 2 | $-0.5 \le x \le -0.25$ | *Obj*(2) | |
| Case 3 | $-0.5 \le x \le -0.38$ | *Obj*(3) | $y(x,z) \ge 0$<br>$\nabla_0 \le \nabla \le 1.05\nabla_0$<br>$y(x,z)_{\max} \le 1.0001 \times \frac{B}{2}$ |

The convergence histories of SQP for each case are shown in Figs.7-9, where $Obj_0$ is the objective functions of the initial hull form and *Obj* is those of optimized hull forms. In the convergence histories of Case 1 and Case 2, *Obj*(1) and *Obj*(2) are reduced together while *Obj*(3) increases. However, the convergence history by *Obj*(3) in Case 3, *Obj*(1) and *Obj*(2) increase while *Obj*(3) is reduced.

The optimization results in Cases 1-3 are summarized in Table 3. The optimization results show that *Obj*(1) is reduced by about 23% in Case 1, *Obj*(2) is reduced by about 4% in Case 2 and *Obj*(3) is reduced by about 3% in Case 3, respectively, compared with the initial hull form. The displacement volumes converge to lower limit given as the respective design constraints for each case.

The comparisons of body plans between the initial and bow optimized hull forms are shown in Fig. 10-12. It is seen that the frame lines of bow of hull forms are distinctly changed from the initial hull form. As shown in Fig. 10 and 11, the change of frame

lines of the optimal hull forms by *Obj*(1) and *Obj*(2) are similar, the bows become a non-protruding bow bulb shape compared with the initial hull form as the frame lines of the bows are shifted inwards in *y*-direction and their displacement volumes move from upper to lower region. However, in Case 3, the obtained hull form by *Obj*(3) is completely different from the other improved hull forms in Cases 1 and 2. The optimal hull has almost the same frame lines as those of the initial hull form except the region very close to the waterline near the free surface as shown in Fig.12.

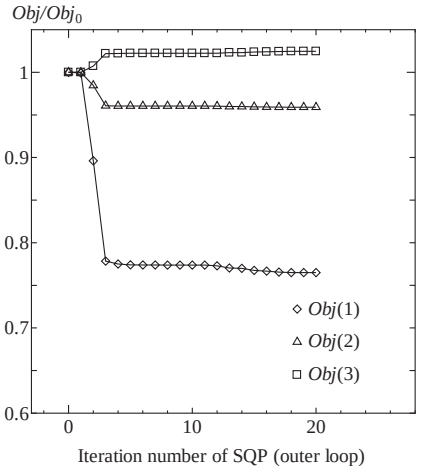


Fig. 7 Convergence history of optimization in Case 1.

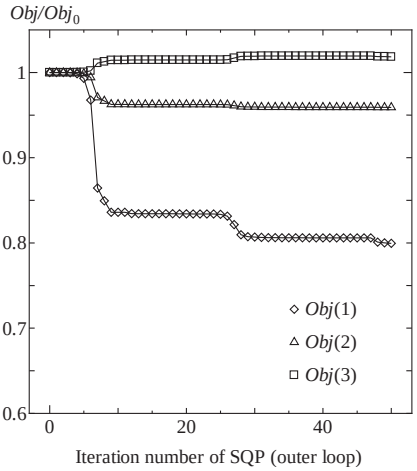


Fig. 8 Convergence history of optimization in Case 2.

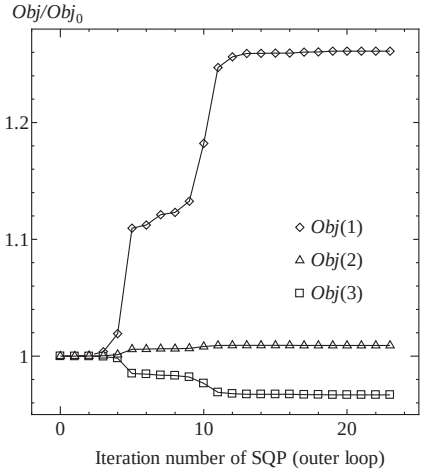


Fig. 9 Convergence history of optimization in Case 3.

Table 3 Results of the optimizations of the ULBS hull form.

| Case No. | Objective functions | $\frac{\nabla}{\nabla_0}$ | $\frac{Obj(1)}{Obj_0(1)}$ | $\frac{Obj(2)}{Obj_0(2)}$ | $\frac{Obj(3)}{Obj_0(3)}$ |
|---|---|---|---|---|---|
| Case 1 | *Obj*(1) | 0.995 | 0.765 | 0.959 | 1.025 |
| Case 2 | *Obj*(2) | 0.995 | 0.800 | 0.959 | 1.018 |
| Case 3 | *Obj*(3) | 1.000 | 1.261 | 1.009 | 0.967 |

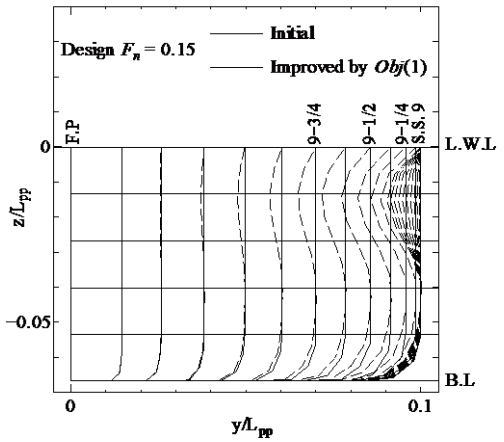


Fig. 10 Comparison of body plans of the initial and improved hull form by *Obj*(1) in Case1.

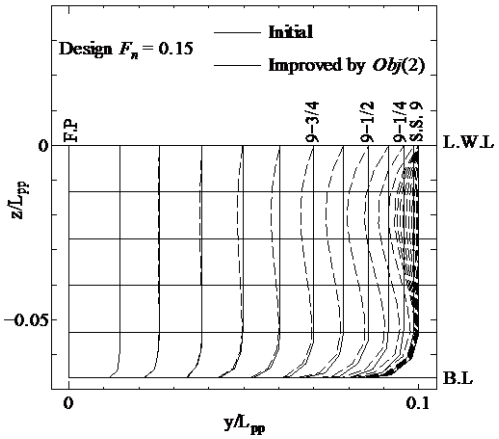


Fig. 11 Comparison of body plans of the initial and improved hull form by *Obj*(2) in Case 2.

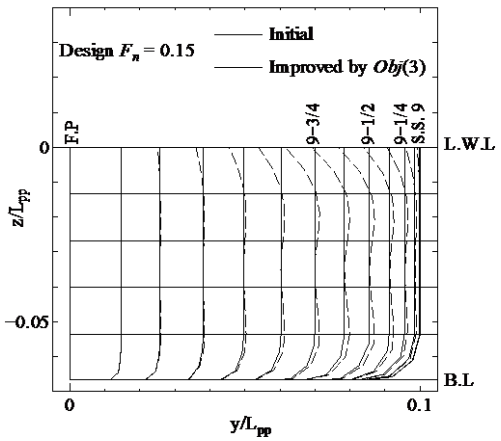


Fig. 12 Comparison of body plans of the initial and improved hull form by *Obj*(3) in Case 3.

The comparisons of the calculated wave profiles on the centerline and along the waterline of the initial and bow optimized hull forms are shown in Fig. 13. Although the difference of bow wave heights between the initial and improved hulls is too small to detect, it is observed that the wave heights in front of the bow of the improved hull forms by *Obj*(1) and *Obj*(2) are actually reduced a little in accordance with the reduction of *Obj*(2) in Cases 1 and 2. As the amount of reduction in *Obj*(2) is the same in both Cases 1 and 2 , the generated wave profile in the improved hull form by *Obj*(1) is very similar to that in *Obj*(2) in front of the bow. The wave heights on the waterline behind the bow are reduced in the improved hulls by *Obj*(1) and *Obj*(2) compared with those of the initial hull form. However, the wave profile of the improved hull form by *Obj*(3) is different from the other improved hull forms because it has almost the same bow wave height as the initial one and the wave heights on the waterline behind the bow become significantly larger than the initial and other improved hull forms by *Obj*(1) and *Obj*(2).

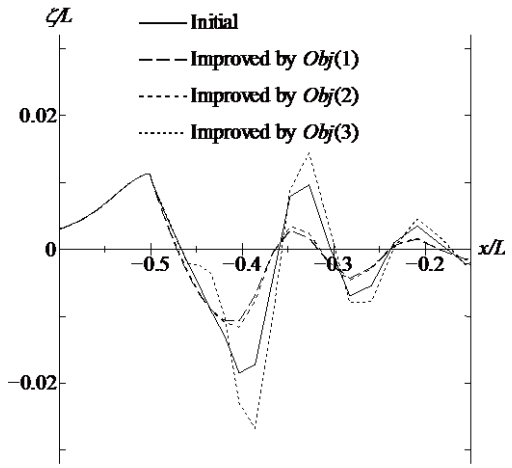


Fig. 13 Comparison of wave profiles on the centerline and along the waterline of the initial and improved hull forms.

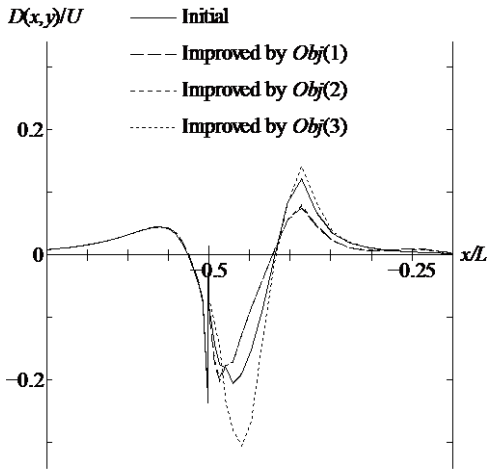


Fig. 14 Comparison of the distributions of $D(x,y)$-values on the centerline and along the waterline of the initial and improved hull forms.

The comparison of the distributions of free surface disturbance function $D(x,y)$-values on the centerline and along the waterline of the initial and improved hull forms are shown in Fig. 14. As shown in Fig. 14, the amount of the difference of the distributions of $D(x,y)$-values in front of the bow of the initial and the improved hull forms is also too small to detect, it is observed that the $D(x,y)$-values in front of the bow of the improved hull form by *Obj*(3) reduces a little as the *Obj*(3) is actually reduced in Case 3. On the other hand, $D(x,y)$-values of the improved hull forms by *Obj*(1) and *Obj*(2) increase a little in front of the bow. It is seen that the distributions of $D(x,y)$-values shown in Fig. 14 shows the similar tendency as wave profiles in Fig. 13. The distributions of free surface $D(x,y)$-values in improved hull forms by *Obj*(1) and those by *Obj*(2) are very similar and smaller on the waterline behind the bow than the initial values. However, in the case of *Obj*(3), it is observed that $D(x,y)$-values on the waterline behind the bow are drastically increased compared with those of the initial and other improved hull forms by *Obj*(1) and *Obj*(2) although *Obj*(3) is reduced in Case 3.

Fig. 15 shows the comparison of wave-making resistance coefficient curves for the initial and bow optimized hull forms. As noted earlier, the wave-making resistance is computed for the fore part of the hull. Compared with the initial hull form, wave-making resistance coefficients of the fore part of the hull of the improved hulls by *Obj*(1) and *Obj*(2) are reduced by 23.5% and 20%, respectively at the design speed and are also smaller over a wide range of speed. On the other hand, wave-making-resistance coefficient of the improved hull form by *Obj*(3) is greatly increased by about 26 % of the original value probably due to the higher peak values of free surface elevations and $D(x,y)$-values on the waterline behind the bow.

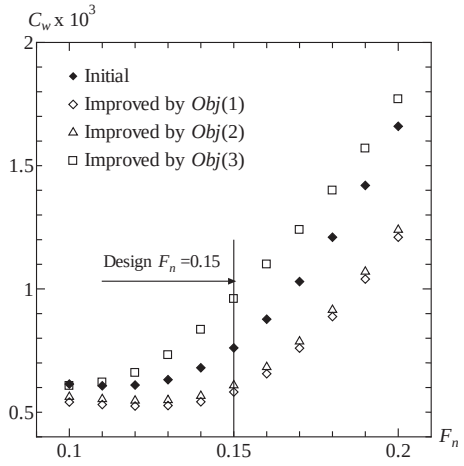


Fig. 15 Comparison of wave-making resistance coefficients of the initial and improved hull forms by Rankine source method.

By summarizing the above optimization results of all Cases 1-3, it is observed that the tendency in optimization results obtained by *Obj*(3) is different from those by *Obj*(1) and *Obj*(2). It is probably because wave-making resistance coefficient and distributions of free surface elevations are evaluated by the Rankine source method with the free surface effect, while free surface disturbance function $D(x,y)$-values are evaluated by the Hess and Smith method[4] based on the double model flow without the free surface effect. Thus, the characteristics of *Obj*(3) are

different from those of *Obj*(1) and *Obj*(2), hence, the tendency in shape deformation and optimization results of *Obj*(3) are also completely different from those of *Obj*(1) and *Obj*(2).

According to the previous results[1], it is expected that *Obj*(3) is effective in the optimization and an optimal hull form can be obtained. However, after optimization, it is found that the optimization process by *Obj*(3) has no good optimal solution since wave-making resistance drastically increases although *Obj*(3) is reduced. It may be caused by the following reasons associated with *Obj*(3):

(1) The free surface effect is not included exactly in *Obj*(3).
(2) The range of the integration domain of *Obj*(3) is only the region in front of the bow .
(3) In the case of full hull forms like ULBS, $D(x, y)$ is sometimes varied rapidly near the bow. In order to get the accurate *Obj*(3), more detailed free surface panels may be necessary near the bow.

## 5. Verification of Optimization Results by CFD Analysis Based on Navier-Stokes (NS) Flow Solver

### 5. 1 Numerical Method

In order to verify the present optimization results, Computational Fluid Dynamics (CFD) based on viscous flow solver is used to estimate the flow characteristics around the initial and bow optimized ULBS hull forms. The flow solver SURF (Solution algorithm for Unstructured RANS with FVM) developed at National Maritime Research Institute[12),13),14)] is employed in this study. An unstructured grid method for simulating three-dimensional incompressible viscous flows is adopted. The incompressible Navier-Stokes equations with artificial compressibility are used as the governing equations. The spatial discretization is based on 2nd order finite volume method for unstructured grid. The backward Euler method is used to carry out the time integration. The Gauss-Seidel iterative method is applied to the linear system derived by the linearization in time. For the analysis of high Reynolds number flows, the $k-\omega-SST$ two-equation turbulence model by Menter[15)] is employed with a wall function approach in the present study.

The comparisons of computational results for viscous flows around the initial and bow optimized ULBS hull forms are presented.

### 5. 2 Computational Conditions

Computational grids are generated for the initial and bow optimized ULBS hull forms by using the commercial code "*Pointwise*". Computational domain is defined by $-1.5 \le x \le 2.5$, $-1.5 \le y \le 0$ and $-1.5 \le z \le 0.5$, while a ship is located at $-0.5 \le x \le 0.5$. Only the port side is discretized due to symmetry. Each grid consists of 4 structured grid blocks and 1,195,200 cells, 1,231,451 nodes and 3,621,504 faces. Grids for the initial and bow optimized hulls of the ULBS are generated to be the same as much as possible in order to reduce the effect of grid difference.

The partial views of computational grids shown in Fig. 16 are the magnified views for bow region of the initial and three bow optimized hull forms obtained by the NLP based on the Rankine source method. Note that the stern grids are almost identical for all hulls. Reynolds number *Re* and Froude number $F_n$ based on the length between perpendiculars $L_{pp}$ which corresponds to a model scale are set to $Re = 4.7 \times 10^5$ and $F_n = 0.15$. The double model flows are also computed for each hull in order to estimate wave-making resistance. The converged solutions with engineering accuracy are obtained with about 2500 iterations for all computational cases.

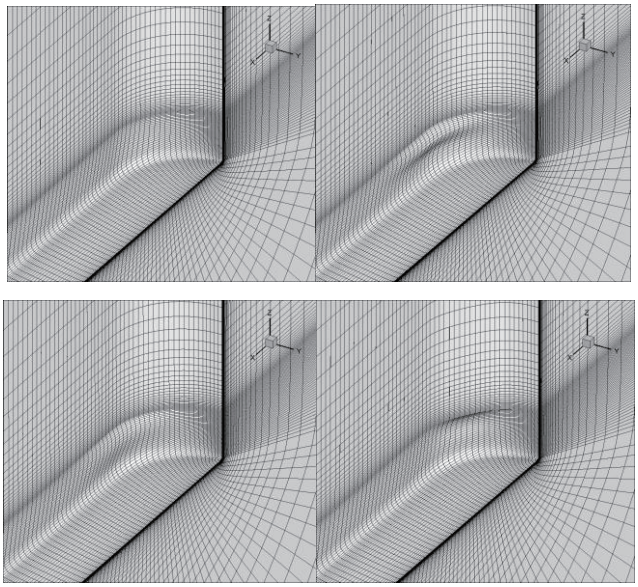

Fig. 16 Partial views of computational grids.
Initial ULBS (top left), Improved by *Obj*(1) (top right)
Improved by *Obj*(2) (bottom left),
Improved by *Obj*(3) (bottom right)

### 5. 3 Simulation Results

The ratios of the coefficients of the computed resistance components of the initial and bow optimized hull forms are shown in Table 4, where $C_t$ ,$C_p$, $C_f$ and $C_w$(fore part) are the coefficients of the resistance components of the improved hull forms and subscript 0 denotes those of the initial hull form.

The wave-making resistance coefficient values of the fore part of the hulls are computed in CFD in order to verify those obtained by the Rankine source method.

The integration of the pressure distributions of the fore part of the initial and improved hulls for both free surface flow and double model flow are computed. The wave-making resistance coefficients of the fore part of the hulls can be evaluated by the difference of pressure resistance coefficients between free surface flow and double model flow.

The comparison of the wave-making resistance coefficients of the fore part of the initial and improved hull forms computed by the Rankine source method and CFD is shown in Fig. 17. Both results of CFD and the Rankine source method show that the wave-making resistance coefficients of the improved hull forms by *Obj*(1) and *Obj*(2) reduce about 20% to 24% of the original value, however, that of improved hull form by *Obj*(3) increases about 12.5 % in CFD and 26% in the Rankine source method from the initial hull. This indicates that the trends of the results of CFD and the Rankine source method are similar. Also as shown in Fig.17, the absolute values of the wave-making resistance

coefficients of the fore part of the hulls of CFD and the Rankine source method do not differ much. Therefore, the wave-making resistance coefficients results of the fore part of the initial and improved hull forms in CFD agree well with those in Rankine source method.

Table 4 Computational resistance components.

| Improved hulls by | Total $\frac{R_t}{\frac{1}{2}\rho U^2 L^2}$ $\frac{C_t}{C_{t0}}$ | Pressure $\frac{R_p}{\frac{1}{2}\rho U^2 L^2}$ $\frac{C_p}{C_{p0}}$ | Friction $\frac{R_f}{\frac{1}{2}\rho U^2 L^2}$ $\frac{C_f}{C_{f0}}$ | Wave-making (fore part) $\frac{R_w}{\frac{1}{2}\rho U^2 L^2}$ $\frac{C_w}{C_{w0}}$ |
|---|---|---|---|---|
| *Obj*(1) | 0.948 | 0.923 | 1.045 | 0.796 |
| *Obj*(2) | 0.946 | 0.919 | 1.054 | 0.779 |
| *Obj*(3) | 0.993 | 1.016 | 0.901 | 1.125 |

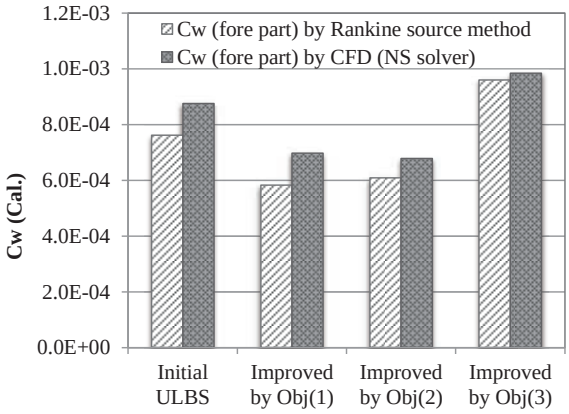


Fig. 17 Comparison of computed wave making resistance coefficients of the fore part of the initial and improved hull forms by Rankine source method and CFD (NS solver).

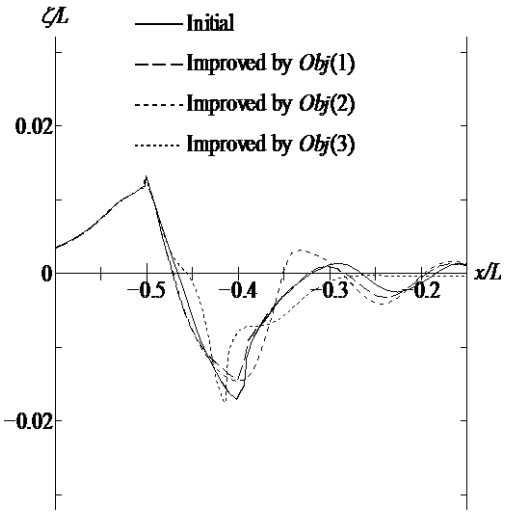


Fig. 18 Comparison of wave profiles on the centerline and along the waterline of the initial and improved hull forms.

The comparison of the computed wave profiles on the centerline and along waterline of the initial and improved hulls are shown in Fig. 18. It is observed that the improved hull forms by *Obj*(1) and *Obj*(2) generate slightly smaller waves than the initial hull form near the shoulders and behind that the waves are similar to those of the initial hull form except the slight discrepancy in the second crest of waves in *Obj*(2). In the case of *Obj*(3), the generated waves are totally different from the initial and other improved hull forms. The wave-breaking is observed at the first trough and behind that the waves become much smaller compared with those of the initial and other improved hull forms.

Comparison of wave profiles obtained from CFD in Fig. 18 with those of the Rankine source method in Fig. 13 shows that the magnitudes of the wave heights of the initial and improved hulls are almost the same at the bow and behind that some differences in the magnitude and position of wave crests and peaks over the free surface are observed. Especially, in the case of *Obj*(3), the distinct difference in generated wave profiles between CFD and the Rankine source method are observed at the first trough. The waves in CFD show the occurrence of wave-breaking and the waves behind the bow are smaller than those in the Rankine source method.

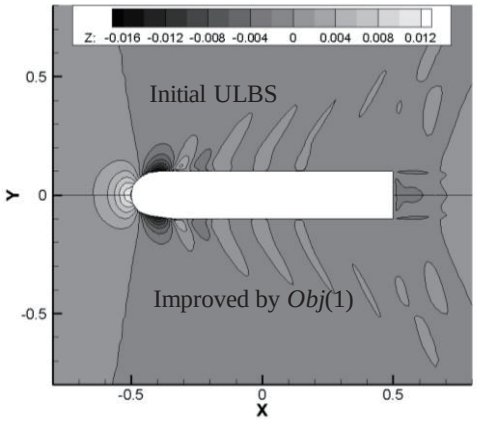


Fig. 19 Comparison of free surface elevation contours of the initial and improved hull form by *Obj*(1).

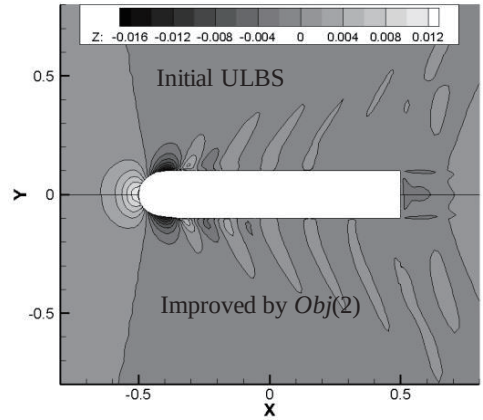


Fig. 20 Comparison of free surface elevation contours of the initial and improved hull form by *Obj*(2).

Figs. 19-21 display the comparisons of free surface elevation contours of the non-dimensional wave patterns calculated for the improved hull forms (lower) and the corresponding wave patterns

of the initial hull (upper) at $F_n = 0.15$, respectively. The figures show the differences in the wave fields generated by the initial and improved hulls. The improved hull form by *Obj*(1) has similar features of wave patterns as the initial hull form and the improved hull form by *Obj*(2) generates slightly larger diverging waves at the far field of the hull. However, in the case of improved hull form by *Obj*(3), the waves show different pattern in the second wave due to the wave-breaking occurred in that region and then diverging waves at the far field become smaller and disappeared.

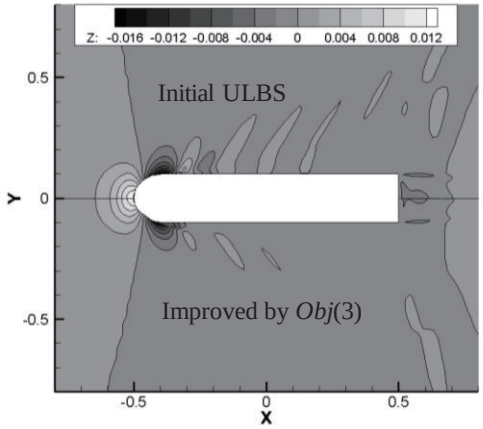


Fig. 21 Comparison of free surface elevation contours of the initial and improved hull form by *Obj*(3).

The magnified view of velocity distributions and streamlines on the free surface around the bow part of the initial and improved hull forms are shown in Figs. 22-25. As it can be seen from the figures, the distinct differences in flow separations due to wave-breaking can be observed which are corresponding to the change of frame lines of the bow part from the initial hull form to the improved hull forms.

In the initial hull form, the separation due to wave-breaking near the shoulder is observed at $-0.4 \le x/L_{pp} \le -0.3$ after the flow fields passing through the round shaped waterline curve of bow smoothly. However, in the case of improved hull form by *Obj*(1), the waterline is modified in the region near the shoulder as the frame lines of optimal hull are shifted inwards in *y*-direction. The flow fields around the bow curve become smoother because of its waterline shape and the separation is smaller than the initial hull form.

The improved hull form by *Obj*(2) has the same tendency in modification as *Obj*(1) and a little reduction of waterline shape from the initial hull form near the shoulder is also observed but the amount of its reduction is smaller than that of *Obj*(1) which keeps the smooth round shaped waterline. It seems the waterline shape of the improved hull by *Obj*(2) is better than those of the initial and *Obj*(1) hull forms as the separation is very weak.

However, in the case of *Obj*(3), the optimal hull has the completely different tendency in modification with the other improved hull forms and the frame lines are changed significantly in the region very close to the still water plane. Such change of frame lines makes the large reduction of width near the water line which yields abrupt change of waterline shape in the region around the shoulder. Thus, a huge flow separation appears near the shoulder which is stronger than that of the initial hull.

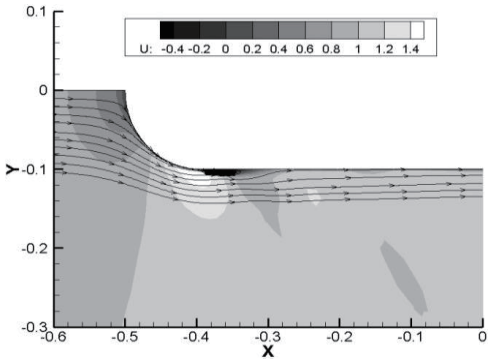


Fig. 22 Velocity distributions and streamlines on the free surface around the bow of the initial hull form.

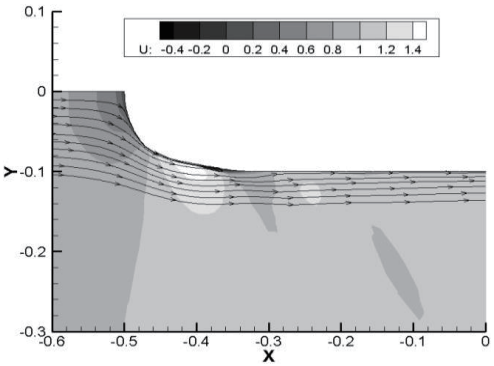


Fig. 23 Velocity distributions and streamlines on the free surface around the bow of the improved hull form by *Obj*(1).

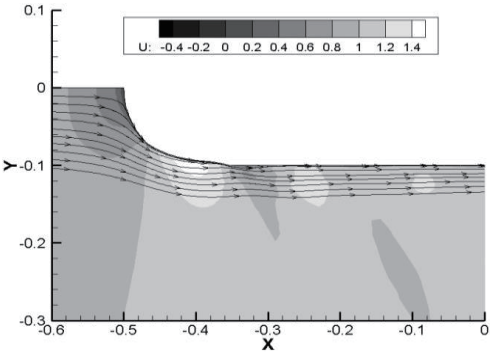


Fig. 24 Velocity distributions and streamlines on the free surface around the bow of the improved hull form by *Obj*(2).

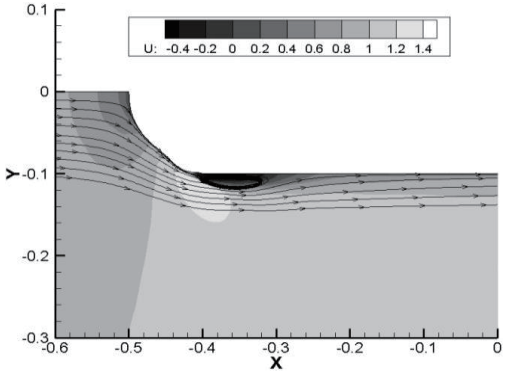


Fig. 25 Velocity distributions and streamlines on the free surface around the bow of the improved hull form by *Obj*(3).

Based on the above results of velocity and streamline distributions around the bow part of the initial and improved hulls, it is observed that the improved hull form by *Obj*(2) produces the weakest separation while the improved hull form by *Obj*(3) produces the strongest separation due to wave-breaking near the shoulders. Thus the intensity of diverging waves shown in Figs. 19-21 can be related to the wave-breaking. The improved hull form by *Obj*(2) with the weakest separation produces the larger diverging waves in the downstream than those of the initial and other improved hull forms because the waves propagate without the significant energy loss due to strong wave-breaking. Also it can be observed that the improved hull form by *Obj*(3) with the strongest separation due to wave-breaking near the shoulder produces the smallest diverging waves in the downstream among the initial and other improved hull forms because the energy dissipation due to wave-breaking makes those diverging waves weaker.

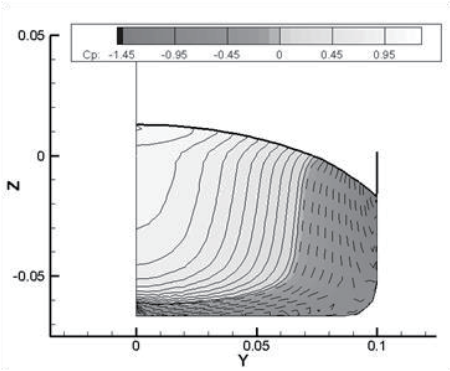


Fig. 26 Hull surface pressure distributions of the initial hull form.

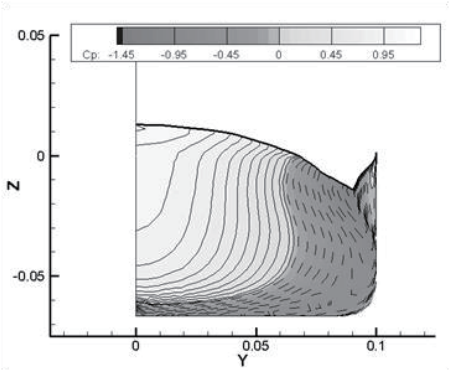


Fig. 27 Hull surface pressure distributions of the improved hull form by *Obj*(1).

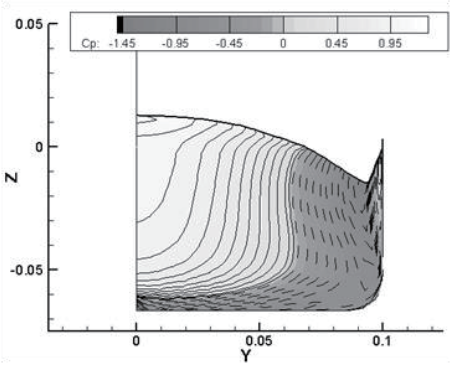


Fig. 28 Hull surface pressure distributions of the improved hull form by *Obj*(2).

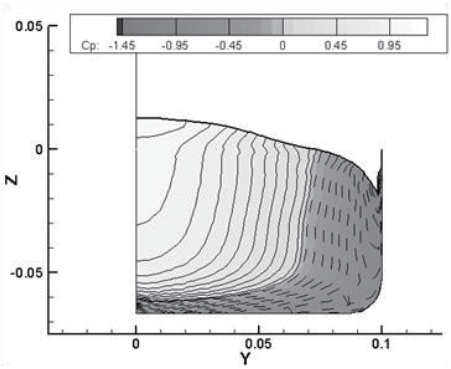


Fig. 29 Hull surface pressure distributions of the improved hull form by *Obj*(3).

The computed hull surface pressure distributions of fore part of the initial and bow optimized hull forms are shown in Figs. 26-29. Only the fore part of the hulls are concerned and aft parts are supposed to be the same. As the pressure is plotted without hydrostatic component, the positive high pressure zone near the bow and the negative low pressure zone near the shoulder can be observed. The positive pressure zone is shown by solid contour lines and negative pressure zone by dashed contour lines. If we focus on the ($y$,$z$) plane of the hull, it can be stated that the distributions of the pressure in this plane are directly related to the pressure resistance. When compared with the pressure distributions of the initial hull form, slight differences are observed in high positive pressure zones but the main differences come from the negative pressure zones near the shoulders in the improved hulls.

In the case of improved hull forms by *Obj*(1) and *Obj*(2), the optimal hulls have the same tendencies in shape deformations where the frame lines are shifted inwards in $y$-direction and the amount of shift in *Obj*(1) is larger than that in *Obj*(2). It is observed that the pressure contour lines are inclined in accordance with the inclination of the frame lines. It is also noted that the amount of the inclination of pressure contour lines in *Obj*(1) is greater than that of *Obj*(2).

Compared with the initial pressure distributions, it can be seen clearly that the negative low pressure zones near the shoulders of the improved hull forms by *Obj*(1) and *Obj*(2) are wider than that of initial hull form while the amounts of positive pressure zones are not so different. Therefore, the integration of pressure on the hull surface is decreased and the pressure resistance is reduced in the improved hulls by *Obj*(1) and *Obj*(2). The amount of reduction of pressure resistance in the improved hull by *Obj*(2) is a little larger than that of *Obj*(1) since the positive pressure zone in *Obj*(1) is a little larger than that of *Obj*(2).

In the case of *Obj*(3), since the optimal hull form has almost the same frame lines as those of the initial hull form except the region very close to the free surface, the vertical pressure contour lines similar to those of the initial hull form are observed. As it can be seen that from Fig. 29, those vertical pressure contour lines produce the narrower negative low pressure zone near the shoulder and the larger positive high pressure zone compared with the initial and other improved hull forms. Thus, the pressure resistance is more increased in the improved hull form by *Obj*(3) than that of the initial and improved hulls by *Obj*(1) and *Obj*(2).

## 6. Conclusions

In the present studies, the bow shape optimization method for minimum wave-making resistance and wave-breaking based on the potential flow solver by the Rankine source method and the NLP is applied to the ULBS hull form ($C_b$=0.9725). The wave-making resistance coefficient, surface integral of the square of free surface elevations and that of free surface disturbance function $D(x, y)$-values are taken as objective functions. The three improved hull forms are obtained by the optimization of bow shape of the hull with minimum objective functions at the design speed $F_n$ =0.15.

In the latter part, verification of the optimization results is made by CFD analysis based on the viscous flow solver. A three-dimensional incompressible Navier-Stokes algorithm based on artificial compressibility is used to compute free surface viscous flows around the initial and bow optimized hull forms. The wave-making resistance coefficients of the fore part of the initial and improved hull forms are computed and compared with each other and with those in the Rankine source method. Both results of CFD and the Rankine source method show that the wave- making resistance coefficients of the improved hull forms by *Obj*(1) and *Obj*(2) reduce about 20% to 24% of the original value, however, that of improved hull form by *Obj*(3) increases about 12.5 % in CFD and 26% in Rankine source method from the initial hull. Therefore, it is confirmed that CFD simulation results based on the viscous flow solver show the same tendency with optimization results based on the potential flow solver by the Rankine source method.

The present study is the first work of hull form optimizations of the full hull form ULBS and the above discussed results indicate that the present optimization algorithm is capable of producing optimal hulls with minimum objective functions. The bow shape optimization procedures based on *Obj*(1) and *Obj*(2) can be accepted as effective design tools for the ULBS as the reduction of wave-making resistance is achieved in a wide speed range. The optimization process by *Obj*(3) might not be applied effectively since the wave-making resistance drastically increases although *Obj*(3) is reduced. It is probably due to the range of integral domain of *Obj*(3). In order to get the accurate *Obj*(3), more detailed free surface panels may be necessary near the bow.

In future works, it is expected that the newer objective functions can be defined by the integration of the disturbance function on the entire free surface or part of the free surface for further understanding of wave breaking characteristics in the ULBS. Further hull form optimizations should be carried out based on the viscous Navier-Stokes (NS) flow solver in order to compare to the present optimization results. It is also expected that the characteristics of the resistance components of the present bow optimized ULBS hull forms can be confirmed by experiments.

## Acknowledgment

The first author acknowledges the Ministry of Education, Culture and Science of Japan (Monbukagakusho) scholarship support for carrying out this research. The authors give thanks to all those who have contributed in accomplishing this research including Mr. Okada of Yokohama National University.

## References

1) Suzuki, K., Md. Ashim Ali, Hino, T., and Aye Aye Mon: Proposal of Ultra Large Block Coefficient Ship and Fundamental Studies on Its Bow Wave Breaking (in Japanese), Journal of the Japan Society of Naval Architects and Ocean Engineers, Vol. 18, pp. 1-7, 2013.
2) Baba, E.: Study on Separation of Resistance Components, Mitsubishi Technical Bulletin, No. 59, 1969.
3) Baba, E.: Blunt Bow Forms and Wave Breaking, The First Ship Technology and Research (STAR) Symposium Washington, The Society of Naval Architects and Marine Engineers, pp. 8-1~8-12, 1975.
4) Hess, A.J., and Smith, A.M.O.: Calculation of Non-Lifting Potential Flow about Arbitrary Three-Dimensional Bodies, Journal of Ship Research, Vol. 8, No.2, pp. 22-44, 1964.
5) Tarafder, M.S., and Suzuki, K.: Numerical Calculation of Free-surface Potential Flow around a Ship Using the Modified Rankine Source Method, Ocean Engineering, No. 35, pp. 536-544, 2008.
6) Suzuki, K., and Iokamori, N.: Studies on the Minimization of Wave resistance Based on the Rankine Source method (in Japanese), Journal of the Society of Naval Architects and Ocean Engineers of Japan, No. 185, pp. 9-19, 1999.
7) Akima, H.: A Method of Bivariate Interpolation and Smooth Surface Fitting for Values Given at Irregularly Distributed Points, ACM Transactions on Mathematical Software, Vol. 4, No. 2, 1978.
8) Akima, H.: On Estimating Partial Derivatives for Bivariate Interpolation of Scattered Data, Rocky Mountain Journal of Mathematics, Vol. 14, No. 1, 1984.
9) Saha G.K., Suzuki, K., Kai, H.: Hydrodynamic Optimization of Ship Hull Forms in Shallow Water, Journal of Marine Science and Technology, Vol. 9, pp. 51-62, 2004.
10) Masuda, S., Suzuki, K., and Kasahara, Y.: An Optimization Method for Full Form Ships Using a Simple Prediction of the Form Factor and Thrust Deduction Factor , Proceedings of PRADS 2004 , Luebeck, Germany, pp. 120-126, 2004.
11) Suzuki, K., Kai, H., and Kashiwabara, S.: Studies on the Optimization of Stern Hull Form Based on a Potential Flow Solver, Journal of Marine Science and Technology, Vol. 10, No. 2, pp. 61-69, 2005.
12) Hino, T.: Navier-Stokes Computations of Ship Flows on Unstructured Grids, Proc. of the 22nd Symp. on Naval Hydro., 1998.
13) Hino, T.: A 3D Unstructured Grid Method for Incompressible Viscous Flows, Journal of the Society of Naval Architects of Japan, Vol. 182, pp. 9-15, 1997.
14) Hino, T.: An Interface Capturing Method for Free surface Flow Computations on Unstructured Grids, Journal of the Society of Naval Architects of Japan, Vol. 186, pp. 177-183, 1999.
15) Menter, F.R.: Two-Equation Eddy-Viscosity Turbulence Models for Engineering Application, AIAA Journal, Vol.32, No.8, pp. 1598-1605, 1994.